AIAA 80-1440R

Experimental Studies of Separation on a Two-Dimensional Airfoil at Low Reynolds Numbers

Thomas J. Mueller* and Stephen M. Batill†
University of Notre Dame, Notre Dame, Ind.

The laminar separation, transition, and turbulent reattachment near the leading edge of a two-dimensional NACA 66_3-018 airfoil were investigated using a low-speed, smoke visualization wind tunnel. Lift and drag force measurements were made using an external strain gage balance for a chord Reynolds number range of 40,000-400,000. An extensive flow visualization study was performed and correlated with the force measurements. Experiments were also conducted with distributed surface roughness at the leading edge and external acoustic excitation to influence the development of the airfoil boundary layer. This study delineates the effects of angle of attack and chord Reynolds number on the separation characteristics and airfoil performance.

Nomenclature

c = model chord
c_d = section profile drag coefficient (uncorrected)
c_ℓ = section lift coefficient (uncorrected)
C_p = pressure coefficient
f = acoustic frequency, Hz
R = reattachment location
R_c = Reynolds number based on chord length, $U_\infty c/\nu$
S = separation location
T = location of approximate end of transition
U_∞ = freestream velocity
x/c = nondimensional distance along chord
α = angle of attack
ν = kinematic viscosity

Introduction

THE performance of airfoils operating in low Reynolds number, incompressible flows has been of increasing interest in the past decade. This interest has been a result of the desire to improve the low-speed performance of general aviation aircraft and high-aspect-ratio sailplane wings, as well as to improve the design of remotely piloted vehicles, jet engine fan blades, and propellers at high altitudes. The inboard sections of helicopter rotors, wind turbine rotors, and free-flying model aircraft also represent applications where low Reynolds number performance is important. Many significant aerodynamic problems appear to occur below chord Reynolds numbers of about 200,000. Although recent advances have been made, there are problems which require more study if further improvements in performance are to be realized. These problems are all related to the management of the airfoil boundary layer.

Initially, this experimental program was focused on a study of the leading-edge separation bubble but it became apparent that separation and transition at other locations on the airfoil also had pronounced effects on the airfoil's performance. Therefore, the results in this paper include effects of the leading-edge separation bubble, as well as other separation and transition phenomena occurring on the airfoil in the low Reynolds number regime.

Presented as Paper 80-1440 at the AIAA 13th Fluid and Plasma Dynamics Conference, Snowmass, Colo., July 14-16, 1980; submitted Sept. 24, 1980; revision received Sept. 14, 1981.

*Professor. Associate Fellow AIAA.
†Assistant Professor. Member AIAA.

A two-dimensional NACA 66_3-018 airfoil section was chosen because it was designed as a laminar airfoil and earlier work had indicated the existence of a separation bubble under certain operating conditions. Direct lift and drag force measurements were made using an external strain gage balance for a chord Reynolds number range of 40,000-400,000. An extensive flow visualization study was performed and correlated with the force measurements. A number of experiments were also conducted using distributed surface roughness at the leading edge and external acoustic excitation to influence the development and behavior of the boundary layer.

Description of the Separation Bubble

The leading-edge separation bubble, shown in Fig. 1, is formed when the laminar boundary layer separates from the surface as a result of the strong adverse pressure gradient downstream of the point of minimum pressure. This separated shear layer is very unstable and transition usually begins a short distance downstream of separation, as a result of the amplification of velocity disturbances present immediately after separation. After transition from laminar to turbulent flow, the turbulent shear stresses energize the shear layer by entraining fluid from the external stream so that it grows rapidly, causing the pressure to rise. Reattachment occurs when the pressure is nearly equal to a value that would exist had there been a turbulent boundary layer over the airfoil with no separation bubble present. The inviscid flow solution value of pressure is also frequently used to determine the reattachment location since it approximates the turbulent boundary-layer case. The region between separation and reattachment is referred to as the separation bubble. Those factors which affect boundary-layer separation also affect the separation bubble and transition in the separated shear layer, namely, thickness of the boundary layer at separation, angle

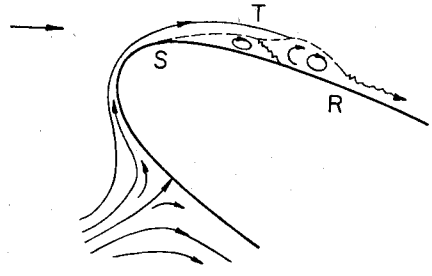

Fig. 1 Laminar separation and turbulent reattachment.

of attack, freestream turbulence level, and/or other freestream disturbances and surface roughness.

The leading-edge separation bubble has been studied for many years.[1-13] Most of these studies have concentrated on one or more of the following effects on bubble characteristics and length: angle of attack, Reynolds number, and freestream turbulence. Separation bubbles have been classified as either short or long. For a short bubble, the length of the turbulent separation shear layer is about the same as the laminar shear layer and the bubble usually extends for only a few percent of the airfoil chord. The long bubble has a turbulent shear layer that extends over most of the airfoil chord with a correspondingly large interaction with the external flow.[12]

At a certain critical value of Reynolds number, the turbulent mixing and entrainment processes which follow the laminar separation can no longer increase pressure to a value high enough for reattachment to occur and to form a short bubble. In this case the peak velocity decreases, resulting in a lower pressure gradient over the bubble. The term associated with this occurrence is bubble "bursting," since the turbulent shear layer reattaches much further downstream to form a long bubble. Long separation bubbles exhibit a surface pressure distribution that has a smoother recovery to the unseparated turbulent boundary-layer value. This gradual pressure rise, together with the reduced minimum pressure peak on the upper surface of the airfoil, is characteristic of long bubbles. Several empirical methods for calculating the characteristics of separation bubbles and obtaining points of reattachment are valid only for short bubbles.[9] For short bubbles, the deviation from the unseparated or inviscid case is small and its effect can essentially be predicted and controlled when calculating flow patterns over airfoils. This situation changes drastically when the bubbles burst into longer ones. Consequently, understanding of the bursting phenomenon is important and much time has been devoted to it.

If the Reynolds number is increased sufficiently, the transition location moves forward of the point where laminar separation would occur. In effect, a turbulent boundary layer is created and this prevents a bubble from forming. This critical Reynolds number is a function of surface roughness, the pressure distribution along the surface in the boundary layer, and the freestream disturbance level. Transition can be the result of "natural" causes or be induced by the placement of a boundary-layer trip near the leading edge of the airfoil. By either means, the surface pressure distribution approaches that of the flow solution for an unseparated turbulent boundary layer, which is approximately equal to the inviscid flow solution.

Experimental Apparatus and Techniques

All experiments were conducted in one of the low-turbulence, subsonic wind tunnels at the University of Notre Dame. The indraft wind tunnel used had 12 antiturbulence screens, followed by a 24/1 contraction in area to the test section. Two identical test sections, 0.61×0.61 m and 1.828 m long, were used.

Airfoil Model

A smooth, two-dimensional NACA 66_3-018 aluminum model was chosen for this study. This 6 series airfoil was designed for laminar flow over a significant portion of its surface. The maximum thickness of this airfoil section occurred at the 45% chord station. The model used in this study had a chord of 0.2489 m, a span of 0.4064 m, and a maximum thickness of 0.0450 m. The model was sprayed with a flat-black paint for the smoke visualization experiments. To study the influence of a rough leading edge, grit was fixed to the leading edge with double-stick tape. The grit was on both the top and bottom surfaces, from the leading edge to approximately 6% of the chord. The grit size distribution was determined using the Tyler screen scale. The grit size distribution by percent total sample weight was found to be as follows:

	0.98% >	0.8407 mm diam
0.8407 mm diam >	40% >	0.5892 mm diam
0.5892 mm diam >	59% >	0.4191 mm diam
0.4191 mm diam >	0.02% >	0.2971 mm diam

Wind Tunnel: Balance Configuration

The lift and drag measurements were made by mounting the airfoil model vertically in the test section and attaching it to an external strain gage platform balance mounted on top of the test section. Two side plates with sharp leading and trailing edges, 0.61×0.61 m, were attached to the upper and lower walls of the test section. Sufficient clearance was left between the ends of the airfoil and the side plates so that the model would not touch these plates during the experiments. The vertical mounting shaft was surrounded by a rigid sheet metal covering the space between the side plate and the top of the tunnel wall so that only the airfoil was subject to the tunnel airflow. The two-component strain gage balance used was specifically designed for measuring small forces. This balance used a dual-flexure system. For very small loads, a flexure capable of measuring forces as low as 0.01 N was engaged. When the load increased toward the upper limit of the first flexure, a second, stiffer flexure automatically engaged. This type of balance yields excellent sensitivity over a wide range of loads. The flexures were instrumented with multiple strain gages. The gage bridge output was amplified using a filter amplifier circuit and recorded on a strip-chart recorder.

The wind tunnel in the standard configuration can produce velocities in the range of approximately 8-27 m/s with a turbulence intensity of about 0.10% over the entire velocity range. The low end of the low Reynolds number range was obtained by inserting a device similar to a flow straightener between the test section and the diffuser. This additional section was filled with plastic drinking straws ($\simeq$5 mm i.d. and 200 mm long). Two such inserts were made and used. Using both inserts, a minimum velocity of 3 m/s was achieved.

Wind Tunnel: Visualization Configuration

The smoke visualization experiments were performed by mounting the airfoil horizontally in a test section with identical dimensions as the balance test section. For chord Reynolds numbers above about 100,000, the smoke-tube techniques developed by Brown[14] were used. The smoke-wire technique[15] was used for chord Reynolds numbers below 100,000. The model was fitted with 0.61×0.61 m end plates which had provision for mounting a horizontal or vertical smoke-wire ahead of the airfoil leading edge.

The horizontal wire was used to introduce a sheet of fine smoke streaklines in a plane along the span of the airfoil model. The wire was located 65 mm forward of the leading edge of the airfoil and was parallel to the leading edge. The vertical wire was used to produce a sheet of streaklines in a plane normal to the leading edge of the airfoil. This wire was located 430 mm forward of the leading edge of the airfoil.

Acoustic Measurements

Sound was introduced into the test section by a speaker arrangement located about 2 m upstream of the antiturbulent screens. The output of a General Radio 1310B audio oscillator was fed through a Heathkit model WA-P2 preamplifier and its companion model W-SM amplifier into two 16 Ω speakers in parallel. The sound was analyzed using a Bruel and Kjaer model 2111 audio frequency spectrometer, a pistonphone calibrator, and a 12.70 mm diam condenser microphone. The frequency spectra and overall intensity level were determined

using a microphone 0.30 m upstream of the first antiturbulence screen, and 0.38 m upstream and about 0.45 m downstream of the airfoil model in the test section floor for selected sound inputs.

Photography

Still photography of the smoke flow was accomplished using a Graphlex 101×127 mm (4×5 in.) camera, synchronized with three high-intensity General Radio type 1532 strobolumes with 20 μs duration, and Kodak Royal-X pan film. In all of the profile photographs presented in the paper the flow is from left to right, and the black airfoil is silhouetted against a black background. Light reflected from the airfoil surface outlines the profile.

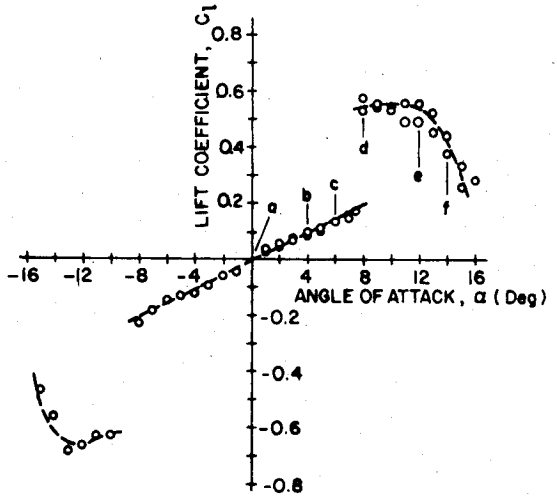

Fig. 2 Lift coefficient vs angle of attack for smooth airfoil at $R_c = 40{,}000$.

Discussion of Experimental Results

The experimental study was conducted over a chord Reynolds number (R_c) range of 40,000-400,000. Primary emphasis was placed on the airfoil's performance at three values of R_c within this range, $R_c \simeq 40{,}000$, 130,000, and 400,000. Each of these three values produced radically different airfoil performance characteristics. The visualization data confirmed that the flow was essentially uniform across the span, except within approximately 25 mm of each end plate.[16]

Due to the complex nature of a number of the phenomena investigated during this experimental program, the following discussion of results will highlight some of the important observations in this continuing research program. This discussion centers on each of the three Reynolds numbers studied.

$R_c = 40{,}000$

The lowest chord Reynolds number studied was approximately 40,000. The lift coefficients vs angles of attack for a number of tests are presented in Fig. 2. The maximum lift force achieved during these tests was approximately 0.3 N (a rather small force). Since the drag forces were more than an order of magnitude smaller, they were not measured at this lowest Reynolds number. A smoke visualization study was also conducted at $R_c \simeq 40{,}000$, and airfoil profile photographs using the smoke-wire technique are shown in Fig. 3 for angles of attack of 0, 4, 6, 8, 12, and 14 deg.

In an attempt to influence the bubble formation, another series of lift force tests was conducted at $R_c \simeq 40{,}000$ with the distributed leading-edge roughness applied to the airfoil. These results are compared with the smooth airfoil results in Fig. 4.

An examination of the visualization photographs (Fig. 3) helps clarify the rather unusual lift characteristics in this very low Reynolds number region. The letters corresponding to the photographs of Fig. 3 are shown in Fig. 2. At zero angle of

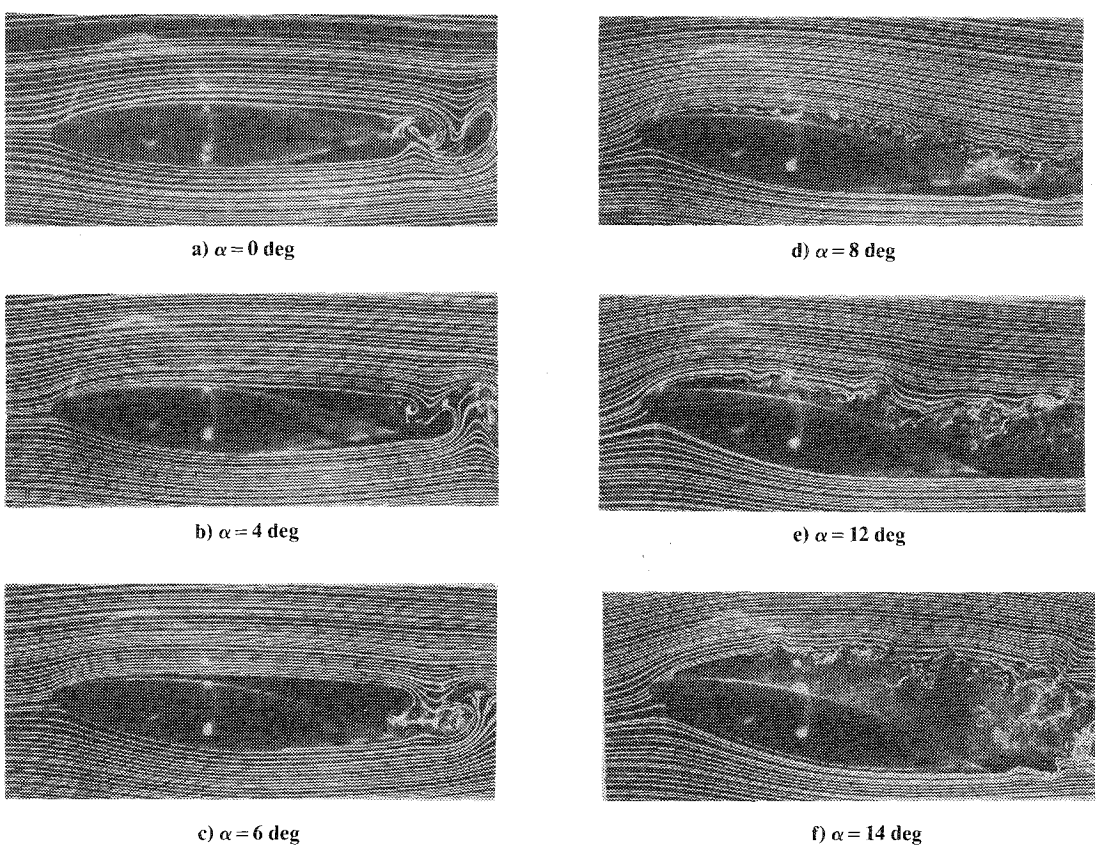

a) $\alpha = 0$ deg

d) $\alpha = 8$ deg

b) $\alpha = 4$ deg

e) $\alpha = 12$ deg

c) $\alpha = 6$ deg

f) $\alpha = 14$ deg

Fig. 3 Smoke-wire visualization for smooth airfoil at $R_c = 40{,}000$, profile view.

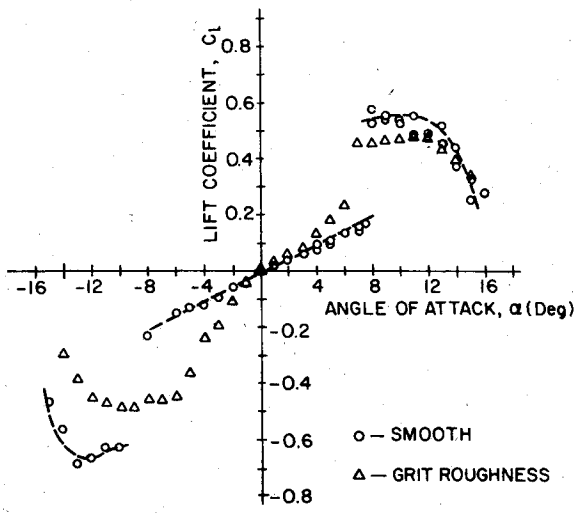

Fig. 4 Lift coefficient vs angle of attack with and without grit roughness at $R_c = 40{,}000$.

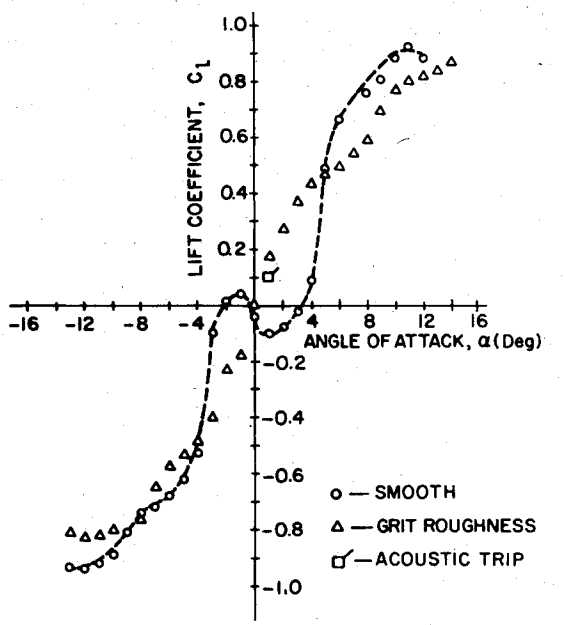

Fig. 5 Lift coefficient vs angle of attack with and without grit roughness at $R_c = 130{,}000$.

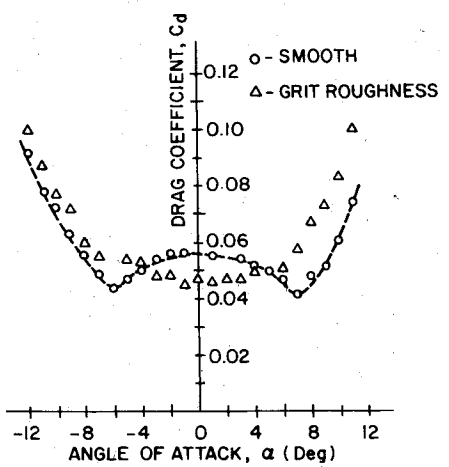

Fig. 6 Drag coefficient vs angle of attack with and without grit roughness at $R_c = 130{,}000$.

attack (Fig. 3a) laminar separation occurs on both the top and bottom surfaces at about 65% chord position. Periodic vortex shedding in the wake is evident. This shedding is characteristic of the wakes of both airfoils and bluff bodies at subcritical Reynolds numbers. The entire flow appears to be laminar. As the angle of attack increases, the lift coefficient increases, but very gradually, since the separation location on the upper surface moves upstream while the separation location on the lower surface moves downstream, e.g., see Figs. 3b and 3c. At $\alpha = 6$ deg (Fig. 3c) the laminar separation on the upper surface is near the leading edge, i.e., somewhere between the 10-15% chord position, while the flow over the lower surface is apparently attached all the way to the trailing edge. The lift coefficient continues to increase with increasing angle of attack until the laminar separation bubble is formed at about $\alpha = 8$ deg (Fig. 3d). Because the separation bubble acts similarly to a trip, inducing transition and a subsequent turbulent reattachment to the airfoil surface, the lift coefficient increases markedly at this point, as shown in Fig. 2. There is, however, a turbulent trailing-edge separation which limits the increase in lift. As the angle of attack continues to increase, this turbulent separation moves upstream (Fig. 3e) until the upper surface is entirely stalled (Fig. 3f) and the lift coefficient decreases rapidly.

Since laminar separation and/or transition are extremely sensitive, even a small change in the surface roughness of the airfoil model would be expected to affect these phenomena. The overall effect of this leading-edge roughness was a more rapid rise in the lift coefficient curve, an earlier formation of the leading-edge separation bubble, and a lower maximum lift coefficient, as indicated in Fig. 4. Since only a single type and size of roughness was used, it is difficult to draw any general conclusion with regard to surface roughness at this low Reynolds number.

$R_c = 130{,}000$

Some of the most interesting results achieved in this study were for a chord Reynolds number of approximately 130,000. The lift and drag coefficients vs angle of attack data are presented in Figs. 5 and 6. The unusual behavior of the airfoil is particularly evident in the angle-of-attack range from -4 to $+4$ deg. Since the freestream velocity exceeds the allowable range for the smoke-wire technique, the visualization data at this Reynolds number were acquired using Brown's technique.[14] Photographs for the smooth airfoil at $\alpha = -2$, 0, 1, 2, and 8 deg are shown in Fig. 7.

The unusual behavior observed at this Reynolds number was not directly related to the laminar separation bubble. Again, the visualization data provided the key to help in understanding the rather atypical behavior of the airfoil. Note that at $\alpha = 0$ deg for the smooth airfoil (Fig. 7b), a laminar separation appears to occur at approximately 65% of the chord on both top and bottom surfaces. As α is increased to 1 deg (Fig. 7c), the separation points shift, the upper surface separation point moving forward and the lower surface point moving aft slightly. Obviously, the Kutta condition is not satisfied at this small angle of attack; in actuality, a net negative circulation is developed because for $0 \lesssim \alpha \lesssim 4$ deg there is negative lift at positive angles of attack. When $\alpha = 8$ deg, transition has occurred on the upper surface and the attached turbulent boundary layer allows for a "normal" development of lift on the airfoil. Although not apparent in this photograph, the surface oil flow study confirms the existence of the separation bubble at $\alpha = 8$ deg. The laminar separation bubble is evident at $\alpha = 12$ deg and influences the high-angle-of-attack performance of the airfoil.

Figure 5 clearly shows an asymmetry in the lift curve, particularly at small angles of attack. Although care was taken to insure a symmetric airfoil section, the airfoil was not perfectly symmetrical. The model was milled from a solid aluminum block but the final surface finish was done by hand and there are very slight surface irregularities on the order of

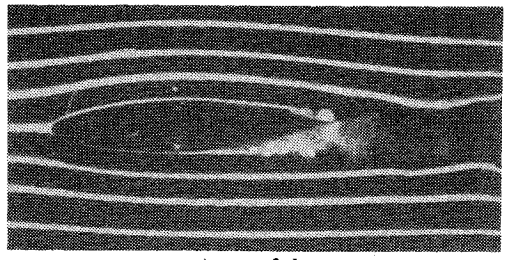

a) $\alpha = -2$ deg

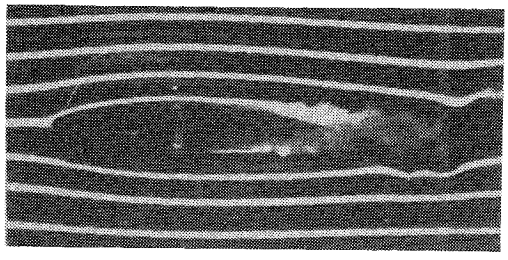

b) $\alpha = 0$ deg

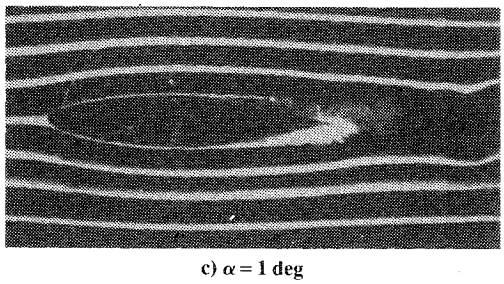

c) $\alpha = 1$ deg

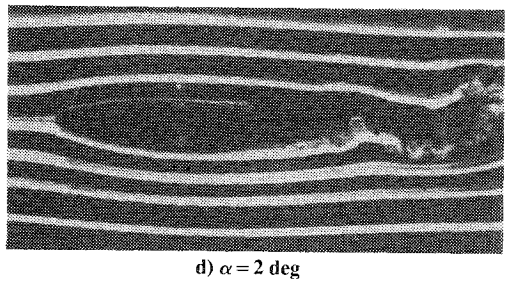

d) $\alpha = 2$ deg

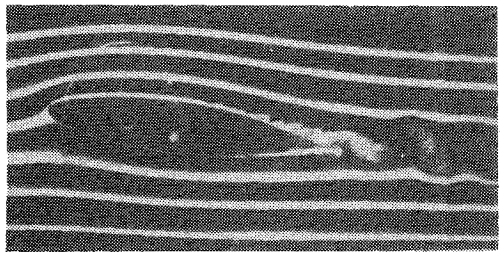

e) $\alpha = 8$ deg

Fig. 7 Smoke visualization for smooth airfoil at $R_c = 130{,}000$, profile view.

0.0015 mm. At this Reynolds number, the asymmetry is apparent, whereas at the other values of R_c tested, where the development of the boundary layer is not so critical, the asymmetry is not obvious.

Due to the unusual behavior of the airfoil, particularly in the low-angle-of-attack range, additional tests were conducted in an attempt to influence the boundary-layer behavior. The distributed leading-edge roughness was used and lift and drag results compare with the smooth airfoil in Figs. 5 and 6. Visualization data were also collected for the roughness model for angles of attack of 0, 1, 8, and 12 deg.[16]

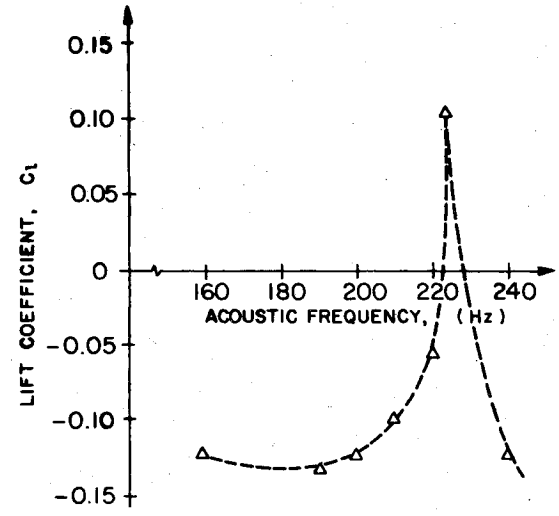

Fig. 8 Lift coefficient vs acoustic frequency for $\alpha = 1$ deg and $R_c = 130{,}000$.

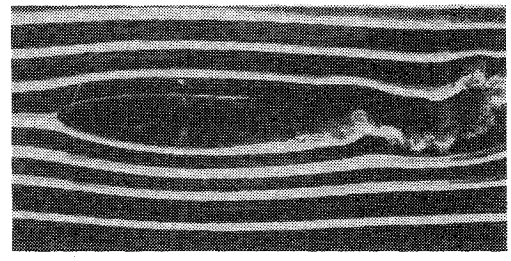

a) No sound

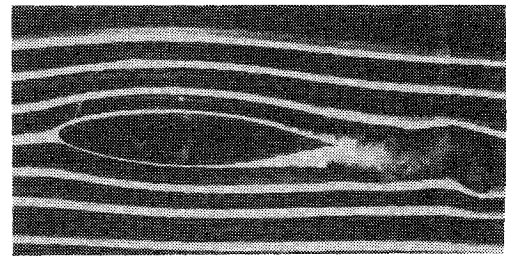

b) 388 Hz

Fig. 9 Smoke visualization with and without sound at $\alpha = 2$ deg and $R_c = 130{,}000$.

External acoustic excitation of the boundary layer was also attempted. Using the equipment described earlier, sound was introduced into the tunnel to modify the boundary-layer development. Audio frequencies of 100-2000 Hz were used and the lift forces monitored as the frequency was changed. The influence on c_ℓ for $\alpha = 1$ deg in the vicinity of 200 Hz ($\simeq$ 100 dB) is shown in Fig. 8. There appeared to be a number of frequencies at which the airfoil flowfield was significantly altered by the acoustic excitation. Visualization photographs comparing the $\alpha = 2$ deg condition, with and without sound at 388 Hz (110 dB), are shown in Fig. 9. A single data point showing the influence of the sound on the lift coefficient at $\alpha = 1$ deg is also included in Fig. 5.

Both the distributed surface roughness and external acoustic excitation alter the development of the boundary layer and change the smooth airfoil performance. The visualization data with the surface roughness at $\alpha = 0$ deg shows an attached turbulent boundary layer over the latter portion of the airfoil. Although the roughness is distributed only over the first 6% of the chord of the airfoil and the apparent transition occurs at about 75% chord, the laminar separation characteristics of the smooth airfoil are avoided.

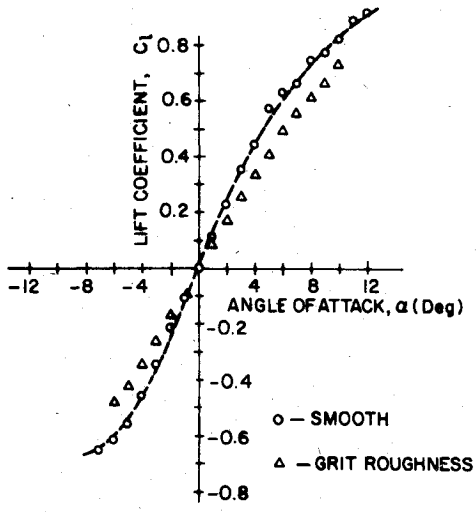

Fig. 10 Lift coefficient vs angle of attack with and without grit roughness at $R_c = 400{,}000$.

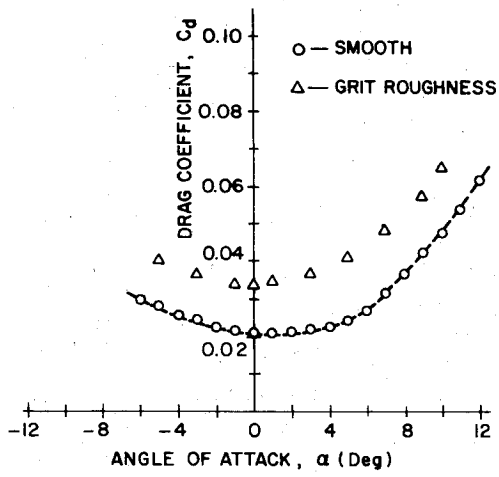

Fig. 11 Drag coefficient vs angle of attack with and without grit roughness at $R_c = 400{,}000$.

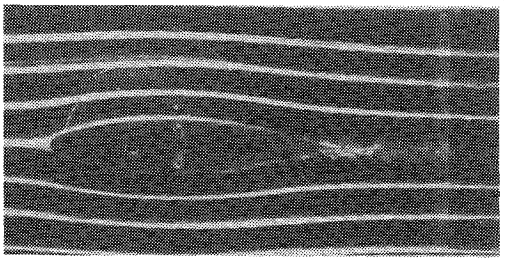

a) $\alpha = 0$ deg

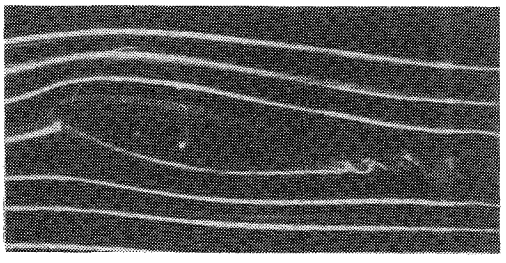

b) $\alpha = 12$ deg

Fig. 12 Smoke visualization for smooth airfoil at $R_c = 400{,}000$, profile view.

As α is increased to 1 deg, the asymmetric laminar separation is not present and positive lift is developed. It should be noted that, whereas the smoke-wire visualization technique yielded significant detail near the airfoil surface, the thicker smoke filaments provide a less detailed picture of the flow near the surface and the percent chord locations mentioned in the previous discussion are only approximate.

The influence of the external acoustic excitation is quite apparent when comparing the photographs in Fig. 9. Although there were a number of audio frequencies which modified the low-angle-of-attack characteristics, the results with 222 and 388 Hz are presented in this paper. With the airfoil mounted on the balance, the frequency range near 220 Hz for an angle of attack of 1 deg was of particular interest, as shown in Fig. 8. By acoustically "tripping" the boundary layer, the lift reversal at $\alpha = 1$ deg was eliminated and the value of c_ℓ is comparable to that for the distributed surface roughness. The actual influence of the sound on the boundary layer is beyond the scope of this paper but similar effects for high-angle-of-attack performance near stall have been recognized for years. The visualization data confirm the results of the force measurements. Without sound at $\alpha = 2$ deg (Fig. 9a), a laminar separation occurs on the top surface at approximately 65% of the chord. The addition of sound (this time at 388 Hz) influences the upper surface boundary layer so that transition appears to occur on the surface and the turbulent boundary layer remains attached over the entire upper surface.

$R_c = 400{,}000$

The final chord Reynolds number studied was to provide the "upper" limit for the series of low Reynolds number tests. The lift and drag coefficient data for this Reynolds number are presented in Figs. 10 and 11 for both the smooth airfoil and the distributed roughness case. Visualization data for the smooth case is given in Fig. 12.

This value of chord Reynolds number does provide typical low Reynolds number performance. Again, both smooth and distributed roughness cases were tested. For the smooth airfoil, the surface oil flow results confirm the presence of a very short ($\simeq 3\%$ chord), separation bubble very near the leading edge at angles of attack greater than about 8 deg. The bubble appears to have an effect similar to that of the surface roughness at the high angles of attack; it promotes transition of the boundary layer and allows the flow to remain attached to higher angles of attack. There are few differences in the lift characteristics of the two cases but the drag data show marked increases in the drag of the "rough" airfoil. The presence of surface roughness, and therefore an attached turbulent boundary layer, results in a marked increase in the drag coefficient in the angles of attack tested.

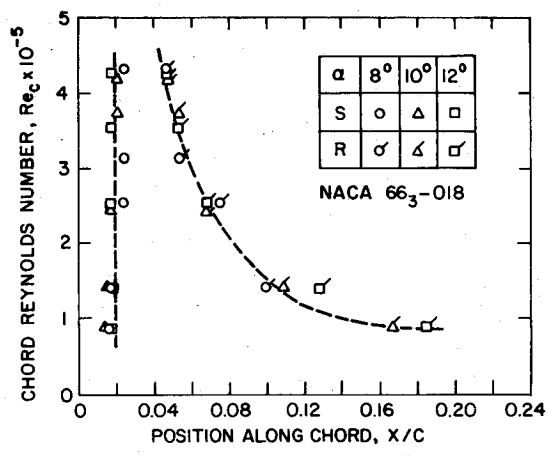

Fig. 13 Separation and reattachment locations vs x/c, surface oil flow test.

Separation Bubble—Surface Oil Flow

Finally, tests were conducted to provide approximate extents of the separation bubble over the entire Reynolds number range considered. Using surface oil flow techniques (titanium dioxide dissolved in the very light bearing oil), the points of separation (S) and reattachment (R) were determined. These data are presented in Fig. 13. The locations of the points of separation and reattachment were measured directly using a scale applied to the airfoil in the tunnel. The data shown in Fig. 13 compare quantitatively with those results observed using the smoke flow visualization. They do indicate the "lengthening" of the short bubble with decreasing Reynolds number and a more apparent dependence on angle of attack at Reynolds numbers below 250,000. The results are also somewhat quantitative since the fluid used for the oil flow may itself affect the boundary-layer development. A more complete and detailed study of the bubble formation using surface pressure measurements is planned.

Conclusions

The correlation of lift-drag measurements with smoke flow visualization data provide a mechanism for understanding the effects of boundary-layer behavior on the overall airfoil performance at low Reynolds numbers.

At $R_c \simeq 40{,}000$, a leading-edge separation bubble forms on the smooth NACA 66_3-018 airfoil at $\alpha \simeq 8$ deg and induces transition which accounts for a sudden increase in lift. Distributed grit roughness on the leading edge produces a more rapid rise in lift with increasing angle of attack than for the smooth case. With the roughness, the leading-edge separation bubble forms at $\alpha \simeq 8$ deg. The $c_{\ell_{max}}$ is less with the roughness than for the smooth airfoil.

The lift vs angle of attack behavior at $R_c \simeq 130{,}000$ was found to be somewhat unusual. At small angles of attack (i.e., between 0 and 4 deg), a negative lift is produced as a result of the location of laminar separation on upper and lower surfaces downstream of midchord. This unusual behavior was eliminated by inducing transition either with grit roughness at the leading edge or by acoustic "tripping." It should be noted that this type of unusual airfoil behavior at these low Reynolds numbers should be highly sensitive to the section shape, particularly the leading-edge geometry, so the results presented in this work should not be considered representative of all airfoils in this R_c regime.

The lift-drag characteristics at $R_c \simeq 400{,}000$ are similar to those expected at high Reynolds numbers. The leading-edge separation bubble on the smooth airfoil, which appears at about $\alpha = 8$ deg, has an effect similar to that for the grit roughness; it promotes transition and, thus, allows the flow to remain attached for large angles of attack.

Acknowledgments

This research was sponsored by NASA Langley Research Center under Grant NSG-1419.

The authors would like to thank Dr. M. V. Morkovin of the Illinois Institute of Technology for his assistance and comments during the acoustic tripping experiments, and Dr. R. C. Nelson for his comments on the revised manuscripts. The efforts of H. Ackert in preparing the figures, B. Jansen Jr. in helping collect the data, D. Balkin in measuring the grit, and Dr. R. Brach in making the acoustic measurements are also acknowledged.

References

[1] Maekawa, T. and Atsumi, S., "Transition Caused by Laminar Flow Separation," NACA-TM-1352, 1952.

[2] Berry, D. T., "A Visual Investigation of Laminar Separation and Turbulent Rejoining of the Boundary Layer as Affected by Angle of Attack," M.S. Thesis, University of Notre Dame, Notre Dame, Ind., 1955.

[3] Gault, D. E., "An Experimental Investigation of Regions of Separated Laminar Flow," NACA-TN-3505, Sept. 1955.

[4] Crabtree, L. F., "Effects of Leading Edge Separation on Thin Wings in Two-Dimensional Incompressible Flow," *Journal of Aeronautical Sciences*, Vol. 24, Aug. 1957.

[5] Ward, J. R., "The Behavior and Effects of Laminar Separation Bubbles on Airfoils in Incompressible Flow," *Journal of the Royal Aeronautical Society*, Vol. 67, Dec. 1963, pp. 783-790.

[6] Tani, I., "Low Speed Flows Involving Bubble Separations," Aeronautical Research Institute, University of Tokyo, *Progress in Aeronautical Sciences*, Vol. 5, MacMillan Co., New York, 1964.

[7] Gaster, M., "The Structure and Behavior of Laminar Separation Bubbles," ARC R&M No. 3595, 1967.

[8] Woodward, D. C., "An Investigation of the Parameters Controlling the Behavior of Laminar Separation Bubbles," RAE Tech. Memo. Aero. 1003, F.M. 3888, 1967.

[9] Horton, H. P., "Laminar Separation Bubbles in Two and Three-Dimensional Incompressible Flows," Ph.D. Dissertation, University of London (Queen Mary College), London, 1968.

[10] Dobbinga, E., von Ingen, J. L., and Kooi, J. W., "Some Research on Two-Dimensional Laminar Separation Bubbles," *Fluid Dynamics of Stall*, AGARD-CP-102, Nov. 1972, pp. 2-1 to 2-8.

[11] Roberts, W. B., "A Study of the Effect of Reynolds Number and Laminar Separation Bubbles on the Flow through Axial Compressor Cascades," D.Sc. Dissertation, von Kármán Institute, 1973.

[12] Young, A. D., "Some Special Boundary Layer Problems," *Z. Flugwiss Weltraumforsch*, Vol. 1, Heft 6, 1977, pp. 401-404.

[13] Arena, A. V. and Mueller, T. J., "Laminar Separation, Transition and Turbulent Reattachment Near the Leading Edge of Airfoils," *AIAA Journal*, Vol. 18, July 1980, pp. 747-753.

[14] Mueller, T. J., "On the Historical Development of Apparatus and Techniques for Smoke Visualization of Subsonic and Supersonic Flows," AIAA Paper 80-0420, March 1980.

[15] Batill, S. M. and Mueller, T. J., "Visualization of Transition in the Flow over an Airfoil Using the Smoke-Wire Technique," *AIAA Journal*, Vol. 19, March 1981, pp. 340-345.

[16] Mueller, T. J. and Batill, S. M., "Experimental Studies of the Laminar Separation Bubble on a Two-Dimensional Airfoil at Low Reynolds Numbers," AIAA Paper 80-1440, July 1980.